Journal of Visualization, Vol. 10, No. 4 (2007)381-388

Regular Paper

Visualizations of the Transitional Flow Patterns at the Mid-Span between Shrouded Co-Rotating Disks

Kong, D -W.*[1], Joo, W -G.*[2] and Doh, D -H.*[3]

*1 Graduate School of Mechanical Engineering, Yonsei University, Seodaemun-ku Shinchon-dong 134, Seoul 120-749, The Republic of Korea.
*2 School of Mechanical Engineering, Yonsei University, Seoul, The Republic of Korea.
E-mail: joo_wg@yonsei.ac.kr
*3 Department of Mechanical and Information Engineering, Korea Maritime University, Pusan, The Republic of Korea.

Received 17 December 2006
Revised 12 July 2007

Abstract : Transitional air flow patterns at the mid-plane of gap between co-rotating disks in a stationary cylindrical enclosure are visualized under the acceleration condition of disks. The flow visualization is performed using olive oil particles with a laser sheet and CCD camera. On disk spinning-up, the transition flow patterns are clearly observed. The affect of magnitude of acceleration on the onset of transition and the relations of the number of vortex cells in fully turbulent regime of the flow in an outer region of the flow field to the rotating speed are also investigated. The centrifugal effect of particle is evaluated from the comparison with visualization results using hollow glass spheres.

Keywords : Visualization, HDD, Co-rotating disks, Flow transition.

1. Introduction

Understanding of the flow generated by co-rotating disks in a cylindrical enclosure is important in the development of hard disk drives (HDD). Air flow goes through the gap between the disks or between the edge of the disk and enclosure with a particular pattern. This flow has highly unsteady complex structures. A flow driven by a rotating disk may have a small or large oscillatory flow patterns, especially in the outer region within a cylindrical enclosure. A large oscillation of the pressure on the surface of the disk may be a disturbing force that excites the vibrational modes of the flexible disk. The strength of the disturbance due to the oscillating flow grows when the rotating speed increases. To understand the flow disturbances on the disk, the flow patterns near the boundary wall of the disk should be investigated.

An experimental study performed by Abrahamson, et al. (1989) visualized the boundary region between the inner and outer region using a dye method in water. Denissenko (2003) and several other authors revealed via a manifold the patterns of the flow disturbances in similar geometrical configurations. Recently Kubo et al. (2003) visualized the flow fields in the co-rotating disks of an HDD submerged in water using a PIV.

These flow visualizations have been performed for fully turbulent flows in water. The present study tried to visualize the flow transition patterns from laminar to turbulent flows in air, not in water using a digital camera and a pulsed laser.

The studies by Calluaud et al. (2005), Wang et al. (2005), Watanabe et al. (2005) and Noma and Mori (2006) and have carried out for the flow visualizations by dye-emission or particle injection method using PIV. Those methods give us useful information for PIV application to complex flow structure. Cui et al. (2006) estimated the effect of six kinds of glass particles on the jet flow structure visualization. The tracer particle selection is important for revealing flow structure. In present study, two types of particles are used to visualize.

Herrero et al. (1999) presented the boundaries of different flow regimes for the flow between a pair of disks co-rotating in a cylindrical enclosure from 2D and 3D calculation results, as shown in Fig. 1. In their calculations it was assumed that there is no gap between disk tip and the enclosure. In the diagram, the regions I, II and III indicate a steady-axis symmetric flow, a shift-and-reflect symmetry flow with respect to the mid-plane between the disks, and an asymmetric flow, respectively.

To cover full range of flow regime, the present study performs visualizations of the flow under the disk spinning up condition from $Re_R = 4.78 \times 10^3$ (disk rotating speed, $\Omega = 20$ rpm) to $Re_R = 1.38 \times 10^4$ ($\Omega = 58$ rpm) in regime I, and at two constant disk speeds, $Re_R = 2.25 \times 10^4$ ($\Omega = 94$ rpm) and $Re_R = 9.55 \times 10^4$ ($\Omega = 400$ rpm) corresponding to regime II and III respectively.

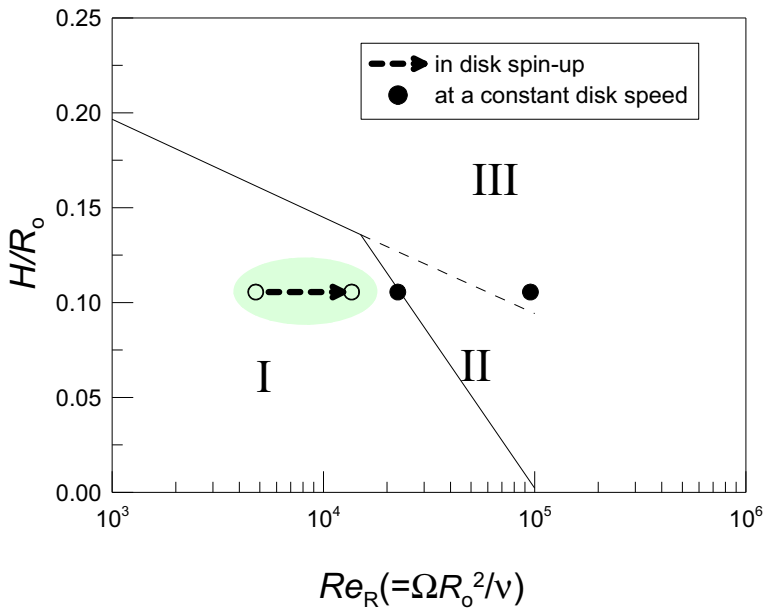

Fig. 1. A range of Re_R for flow visualization in the present study presenting on the qualitative bifurcation diagram (Herrero et al., 1999) for the flow between a pair of disks co-rotating with *no* shroud gap. (R_o: radius of the disk, H: gap distance between the co-rotating disks, Re_R: Reynolds number derived from the angular speed Ω and the outer radius of the disk R_o).

2. Experimental Setup

2.1 Apparatus

A test rig for visualization consists of four co-rotating disks in a fixed cylindrical enclosure. Figure 2 shows a schematic diagram describing this apparatus. The radius of the disk is about four times larger than that of the disk embedded in a recent HDD personal desktop computer. The thickness of the disk is 8 mm. The enclosure wall is made from 5 mm thick transparent Plexiglas pipe by centrifugal tubing. The enclosure top cover is also made of Plexiglas. The top two disks are made of Plexiglas and the other two lower disks are made of steel. An 8 mm hole is drilled to allow the injection of scattering particles. All measurements are performed in the space between the pair of disks at the center. A one horsepower AC motor drives a pair of disks through a coupling.

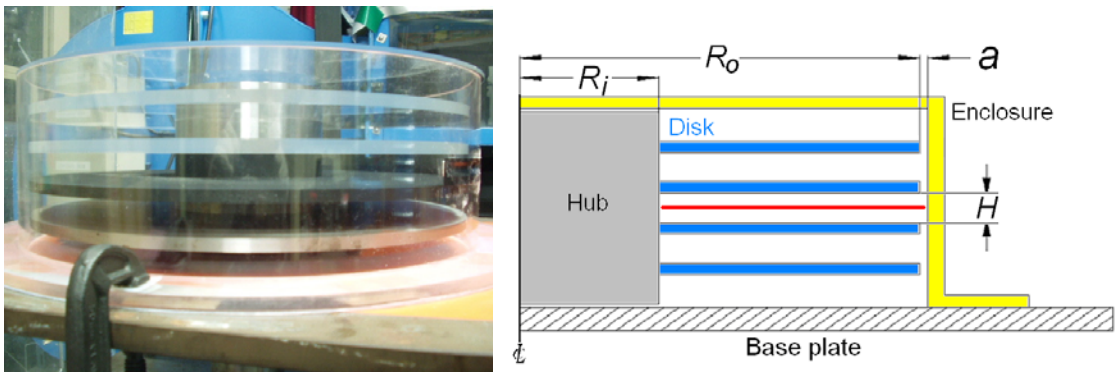

Fig. 2. Schematics of the test rig for visualization; R_o = 190 mm, R_i = 66 mm, a = 5 mm, H = 20 mm.; The flow is visualized at the mid-height between disks (red line).

2.2 Applicability of Particles for Flow Visualization

The small sized olive oil particles generated by a collision type atomizer are used for flow visualization. Figure 3 shows the distribution of olive particle size, which is obtained by the method suggested by Lee et al. (2006). The mean diameter of the scattered particles is approximately 400 nm.

The applicability of the particles to the rotating flow can be evaluated with the drift velocity (u_t) of a particle. When the flow around the particle is laminar, $Re < 0.6$, the terminal free settling velocity of a spherical particle in laminar rotating flow is determined by Eq. (1) derived from the balance of radial forces acting on the sphere particle including the effect of centrifugal acceleration.

$$u_t = \frac{(\rho_p - \rho_a) r \Omega^2 d_p^2}{18 \mu} \quad (1)$$

The drift velocity calculated at the tip radius is 2×10^{-3} m/s (0.007 % of local disk speed) for olive oil particle (density = 920 kg/m^3). The hollow grass spheres are also used to investigate the centrifugal effect of particles. The diameter of the particle is 10 μm and the nominal density is 650 kg/m^3. The calculated drift velocity is 0.9 m/s (3 % of local disk speed). The drift velocity of hollow grass is much higher than one of olive oil. The effect of centrifugal force will be discussed in section 3.4. The terminal velocities of particle in the axial direction due to gravity are 4×10^{-6} m/s for olive oil and 2×10^{-3} m/s for hollow grass and these effects are negligible.

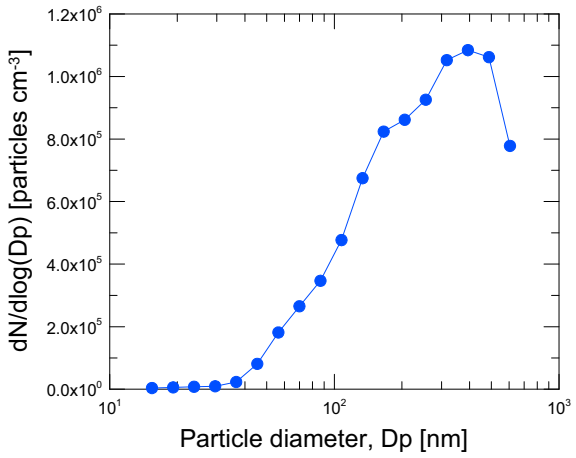

Fig. 3. The distribution of particle size for olive oil from an atomizer.

2.3 Experimental Procedures

The operating fluid is air at a typical room temperature. The measurement system consists of a CCD camera of HiSense MKII (1,344 by 1,024 pixels) with a wide angle lens, an image grabber, and a laser system. Two types of laser systems are used for visualization. An Nd-Yag laser system (15 mJ/pulse) is used for the visualization of olive oil particles, and an argon laser (5W) with AOM is used for the visualization of the hollow glass spheres. The laser control system of each laser and the frame grabber of the camera are synchronized. A laser sheet, passed through a slit 1 mm thick in each case is positioned at the disk's mid-plane. The particles are seeded into the hole on the shroud surface with a particle laden flow rate of 1 l/min with an atomizing pressure of about 4.1×10^5 Pa. As soon as the particles have been seeded, the hole is covered with a flush mounted cap and then the experiment is performed. The frame rate of the image sequence is 11.2 Hz. This frame speed is enough to observe the flow transition during the acceleration of the disks.

The flow field generated by co-rotating disks in a shroud is usually divided into two regions; an inner region where the fluid flows like rigid body rotation and an outer region where the fluid is affected by the shroud wall. Figure 4 shows the distribution of circumferential velocity measured by LDV on the mid-span plane between disks. From the figure, we can clearly see these two regions.
If particles are packed into the shroud when disks are at the rest and then the disks start to rotate, the particles fill the whole flow field so that inner and outer regions can not be distinguished. To visualize these two regions, particles are packed into the shroud while disks are rotating at the lowest possible speed of 20 rpm so that the particles would stay in outer region only.

After seeding particles, the experiments for visualization are performed with increasing the disk rotating speed to investigate the transition from laminar flow to turbulent flow. The disks are accelerated from the starting speed of 20 rpm, corresponding to $Re_R = 4.78 \times 10^3$ to the final speed of 60 rpm, corresponding to $Re_R = 1.43 \times 10^4$ for 30 seconds. This range would be expected to cover the laminar, transitional, and turbulent flow regimes. The flow is visualized at the mid plane of the gap between the second and third disks.

The disk-motor-coupled system used has second order rotational dynamic characteristics. Figure 5 shows the acceleration profiles of the rotational disk system. The experiments are performed at two different acceleration conditions to investigate the effect of acceleration specified in section 3.2. The dots correspond to the visualized results shown in Fig. 6 and in Fig. 7.

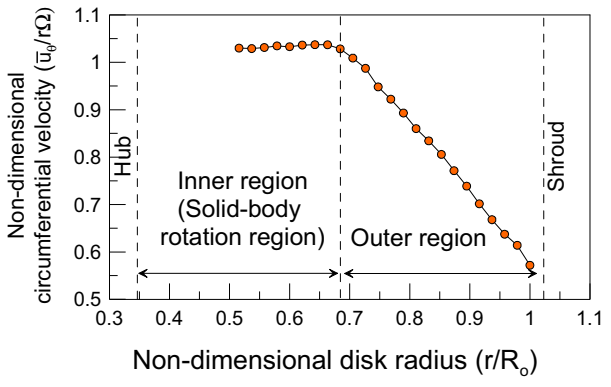

Fig. 4. The distribution of circumferential velocity ($\bar{u}_\theta/r\Omega$) at $Re_R = 2.39 \times 10^4$ at the mid span measured using LDV.

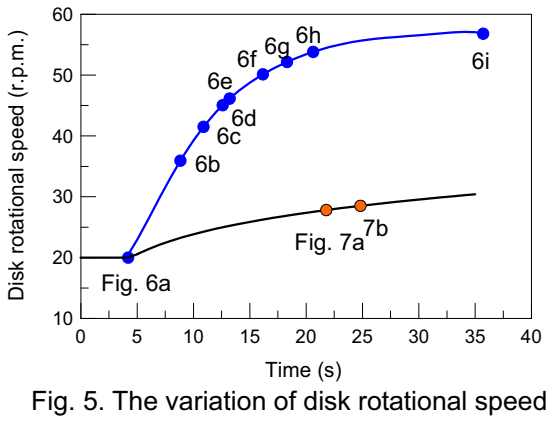

Fig. 5. The variation of disk rotational speed with time.

3. Results and Discussion

3.1 Flow Transition Patterns under Spin-Up Condition

Figure. 6 shows the flow transition pattern during spin-up of the disks. The flow pattern at the lowest speed of 20 rpm (Fig. 6(a)) shows slightly the circumferential periodic Kelvin-Helmholtz type instability at the boundary between the inner and outer regions. This instability pattern is related to the level of disturbances during seeding and the instability becomes stable after finishing seeding.

When the rotational speed of the disks increases more, the small vortex cells start to be generated near the shroud wall (Fig. 6(b)). These vortex cells are developed with increase of the disk speed, and are formed with a radial thickness of approximately 16 percent of the disk radius (Fig. 6(c)). These vortex cells are broken down and mixed, and the radial thickness of the cell region grows inward (Figs. 6(d)-6(f)). The flow in this outer region transits from laminar flow to the turbulent flow with the break down of the vortex cells. At higher speed, the flow in the outer region is fully developed to turbulent flow (Figs. 6(g)-6(h)) and the new big vortex cells of specific number (seven in this case) are developed (Fig. 6(i)), while the flow in the inner region remains laminar rigid body rotation. With the development of new turbulent vortices, the boundary between the inner region and outer region changed from a circular shape to a polygon shape. The particles in the outer region are highly mixed by the development of turbulent flow while the ones in the inner region remained unchanged.

3.2 The Effects of Acceleration

An experiment has been performed to investigate the effect of acceleration. Figure 7 shows the flow visualization when the rotating speed increases to 35 rpm ($Re_R = 8.36 \times 10^3$) for 10 seconds after seeding at the lowest speed of 20 rpm ($Re_R = 4.78 \times 10^3$) as can be seen in Fig. 5. Figure 7(a) shows the onset of generation of small vortex cells near the shroud wall (Fig. 6(b)) and Fig. 7(b) shows the complete formation of the vortex cell (Fig. 6(c)) which still remains at the final speed of 35 rpm. It can be found, from the comparison with Fig. 6, that the flow starts the transition earlier at lower acceleration.

3.3 The Number of Vortex Cell in Fully Turbulent Regime of Outer Region

It has been well known that the boundary between an inner region of rigid body rotation flow and an outer region of the fully turbulent flow in co-rotating disks with a shroud, has the structure of the lobe patterns (Abrahamson et al., 1989), as can be seen in Fig. 6(i). To investigate the effect of disk rotating speed on the number of turbulent vortex cells in the outer region, experiments are performed for the higher speeds, $Re_R = 2.25 \times 10^4$ (Ω = 94 rpm) and $Re_R = 9.55 \times 10^4$ (Ω = 400 rpm). The olive oil particles for flow visualization are injected into the flow at the constant speed after the disk reaches to the specific speed, to obtain a clearer picture.

Figure 8 shows the flows with lobe patterns, as Fig. 6(i) visualized in the spin-up condition. However, the number of vortex cells in the outer region is different with the rotating speed. The number of vortex cells are seven at $Re_R = 1.36 \times 10^4$ (Fig. 6(i)) and six at $Re_R = 2.25 \times 10^4$ (Fig. 8(a)) and five at $Re_R = 9.55 \times 10^4$ (Fig. 8(b)). It can, therefore, be concluded that the number of vortex cells in outer region decreases, as the rotating speed increases.

3.4 Effect of Particle Class in Centrifugal Force on the Boundary Pattern

The flows are visualized using hollow glass spheres (Fig. 9) under the same rotating speeds as the case of flow visualization (Fig. 8) using olive oil particles to evaluate the influence of drift velocity. As shown in Fig. 8 and Fig. 9, in spite of identical Reynolds numbers, the flow visualization images are slightly different with the types of seeding particle. The lobe structures at the boundary between outer and inner regions appear more clearly in the case of the hollow glass spheres than in the case of olive oil particles. It would be because the hollow glass spheres are more influenced by centrifugal forces, as can be seen in section 2.2, so that the hollow glass sphere particles could not permeate into the inner region, where the flow characteristics are completely different, through the layer of a lobe shape.

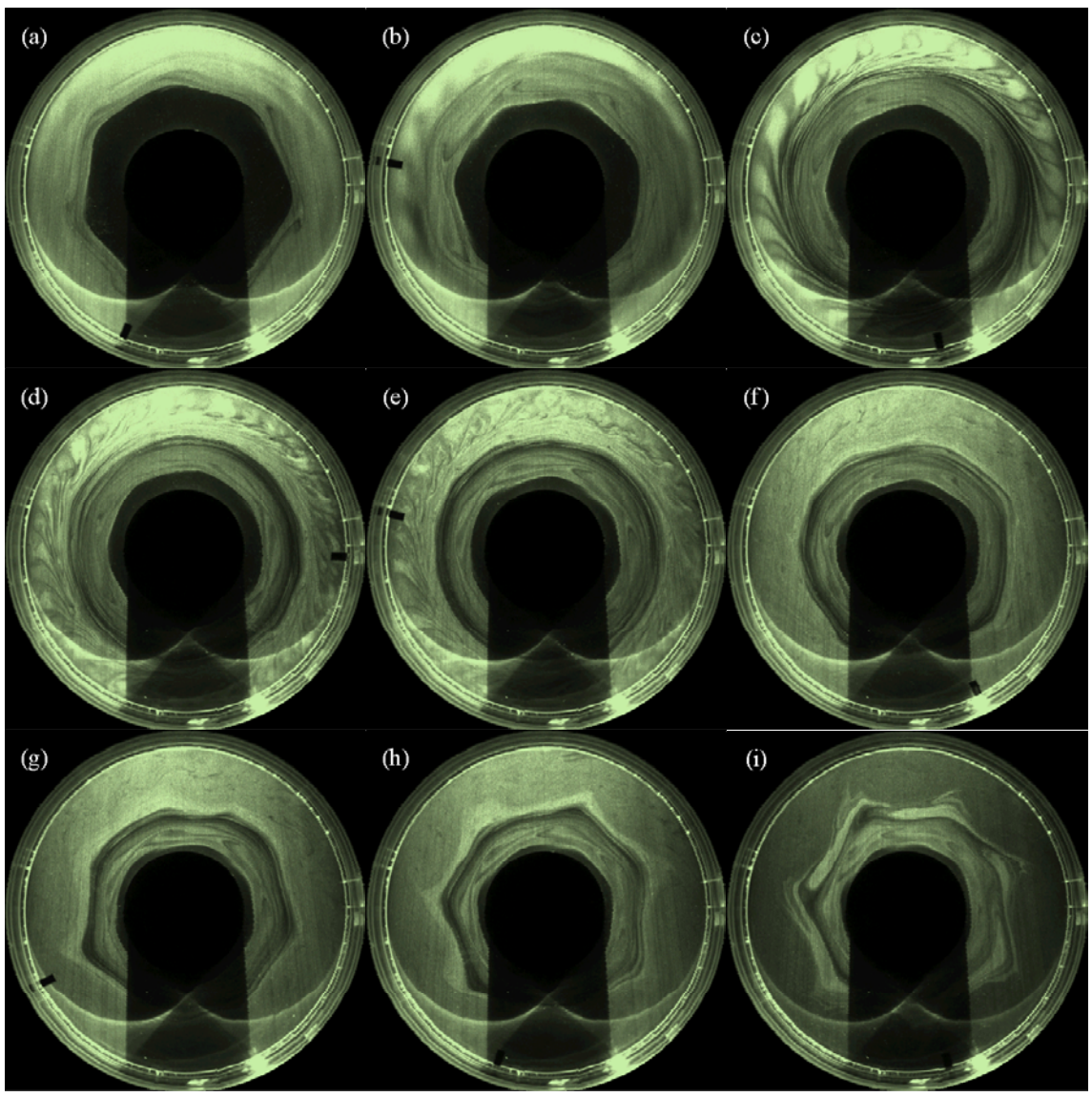

Fig. 6. Flow transition patterns during disk spinning-up; (a) $Re_R = 4.78\times10^3$, (b) $Re_R = 8.58\times10^3$, (c) $Re_R = 9.91\times10^3$, (d) $Re_R = 1.08\times10^4$, (e) $Re_R = 1.10\times10^4$, (f) $Re_R = 1.20\times10^4$, (g) $Re_R = 1.25\times10^4$, (h) $Re_R = 1.29\times10^4$, and (i) $Re_R = 1.36\times10^4$.

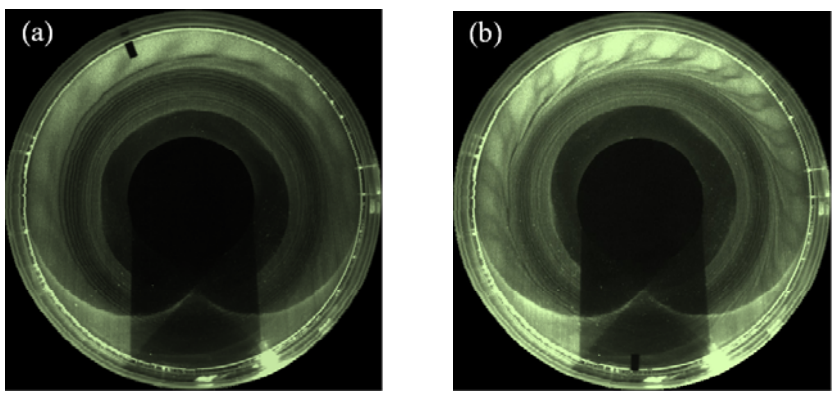

Fig. 7. Flow transition at the lower acceleration condition (a) $Re_R = 6.64\times10^3$, (b) $Re_R = 6.81\times10^3$.

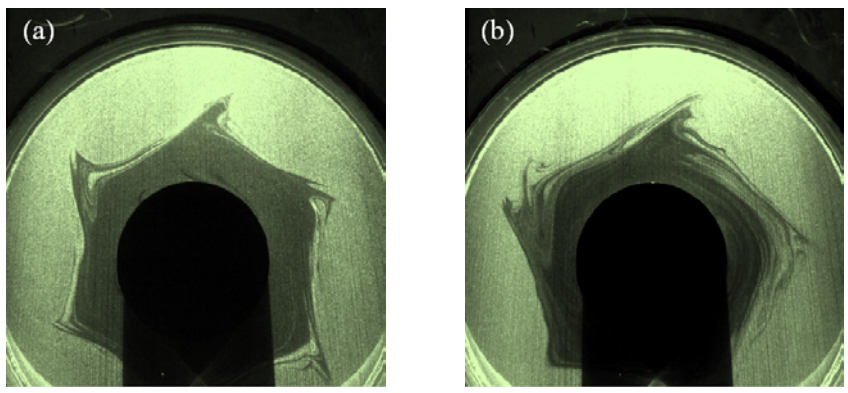

Fig. 8. The fully turbulent flow pattern at a constant disk speed with (a) $Re_R = 2.25\times10^4$, (b) $Re_R = 9.55\times10^4$.

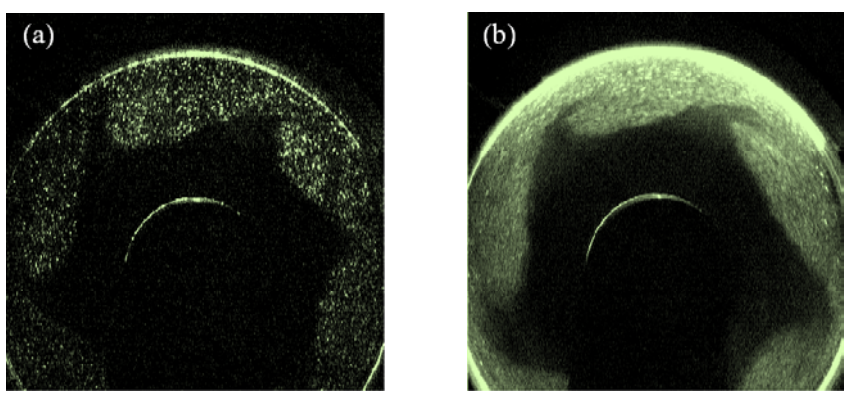

Fig. 9. Flow visualization using hollow glass sphere at (a) $Re_R = 2.25\times10^4$, (b) $Re_R = 9.55\times10^4$ for the comparison with flow visualization using olive oil particles in Fig. 8.

On the other hand, when the particles were less influenced by the centrifugal force, as the case of olive oil particles (Fig. 8), the particles can permeate into the inner region, so that the visualized images cannot show the sharp and clear lobe shape. Therefore if we want to obtain the images with a clear lobe structure, it would be better to use the particles with higher drift velocity which cannot permeate into the inner region by centrifugal force in this case.

4. Conclusion

The transition patterns from laminar to turbulence flow at the mid-span of the gap between co-rotating disks in a shroud are successfully visualized using olive oil particles under the spin-up condition. The flow transition begins with small vortex cells appearing near the shroud wall. These vortex cells are broken down and the flow in the outer region is developed to the turbulent flow with new bigger vortex cells of the specific number, but the flow in the inner region remains laminar solid body rotation. The boundary between the inner and outer region has lobe shape. The number of vortex cells in outer region decreases as the rotating speed increases.

In addition, the onset of transition is affected by the magnitude of acceleration and the flow starts the transition earlier at lower acceleration. The lobe shape of the boundary between the inner and outer regions is more clearly visualized in the case of using the hollow glass spheres by the higher centrifugal force effect than in the case of using olive oil particles.

References

Abrahamson, Scott D., Eaton, John K. and Koga, Dennis J., The flow between shrouded co-rotating disks, Phys. Fluid A, 1-2 (1989), 241-251.

Calluaud, D., David, L. and Texier, A., Vortex shedding process investigation downstream a surface-mounted block, Journal of Visualization, 8-2 (2005), 99-108.

Cui, J. L., Zhang, H. Q., Wang, B., Rong, Y. and Wang, X. L., Flow Visualization and Laser Measurement on Particle Modulation to Gas-Phase Turbulence, Journal of Visualization, 9-3 (2006), 339-345.

Denissenko, Petr Valerievich, Asymmetric Flows Driven by a Rotating Solid in a Fluid Layer, (2003), A dissertation, University of Hull.

Herrero, J., Giralt, F. and Humphrey, J. A. C., Influence of the geometry on the structure of the flow between a pair of corotating disks, Physics of Fluids, 11-1 (1999), 88-96.

Kubo, T., Nishijima, N., Shimizu, H., Hirono, Y., Tokuyama and Nakamura, S., Investigation of Flow Velocity in Actual Hard Disk Drives by Particle-image-velocimetry and Fluid Simulation, JSME-IIP/ASME-ISPS Joint Conference on Micro-mechatronics, (2003), 205-206.

Lee, D. Y., Lee, J., Park, D., Kim, S. Y. and Hwang, J., Sampling and analysis of particles generated in contact start/stop-mode of a hard disk drive by using a particle sampler, Mycrosyst Technol., 12 (2006), 537-544.

Noma, M. and Mori, A., Study on the structures of fluid flows in the annular space formed by a submerged tilting pad journal bearing, Journal of Visualization, 9-4 (2006), 457-465.

Wang, F. H., Jiang, G. D. and Lam, K., Flow patterns of cross-flow around a varicose cylinder, Journal of Visualization, 8-1 (2005), 49-56.

Watanabe, Y., Hashizume, Y. and Fujisawa, N., Simultaneous flow visualization and PIV measurement of turbulent buoyant plume, Journal of Visualization, 8-4 (2005), 293-294.

Author Profile

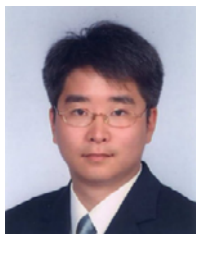

Dae-Wee Kong: He received his B.S. degree in 1998 and M.S. degree in 2001 from Yonsei University, Seoul. He is a Ph.D. candidate in the school of Mechanical Engineering from the same university. He was a research worker at the CISD (Center for Information Storage Device, Seoul) from 2001 to 2005. He is also a student member of ASME. His current research interests are computational fluid dynamics, rotating flow instability, and measurement with PIV.

Won-Gu Joo: He received his B.S. and M.S. degrees in 1978 and 1981 respectively from Mechanical Engineering, Yonsei University. He obtained his Ph.D. at Department of Engineering of University of Cambridge in 1994. He is currently working at Yonsei University in Korea as an associate professor. His current research interests are rotating flows, fluid-structure interaction, and turbomachinery aerodynamics.

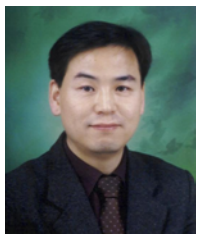

Deug-Hee:Doh: He received B.A. and M.S degrees at Korea Maritime University (KMU) in 1985 and 1988. He obtained his PhD. degree at the Department of Mechanical Engineering of the University of Tokyo, Japan in 1995. His graduate work is on the development of 3D-PTV and simultaneous measurement techniques on temperature and velocity fields for thermal flows. He worked as an invited researcher for the Advanced Fluid Engineering Research Center (AFERC) in 1995. He has been working for Korea Maritime University since 1995 at the Division of Mechanical and Information Engineering. His research interests are to develop spatial measurement techniques such as 3D-PIVs, 3D-PTVs, micro-4D-PIV/4D-PTV for nano-/bio- flows.